Optical Breath Gas Sensor for Extravehicular Activity Application

William R. Wood,[1] Miguel. E. Casias,[2] Andrei B. Vakhtin,[3] and Jeffrey S. Pilgrim[4]
Vista Photonics, Inc., Santa Fe, New Mexico 87508-9463

Cinda Chullen[5]
NASA Johnson Space Center, Houston, Texas, 77058

Eric A. Falconi[6]
GeoControls Systems, Inc., Houston, Texas, 77058

and

Summer McMillin[7]
Jacobs, Houston, Texas, 77058

The function of the infrared gas transducer used during extravehicular activity in the current space suit is to measure and report the concentration of carbon dioxide (CO_2) in the ventilation loop. The next generation portable life support system (PLSS) requires next generation CO_2 sensing technology with performance beyond that presently in use on the Space Shuttle/International Space Station extravehicular mobility unit (EMU). Accommodation within space suits demands that optical sensors meet stringent size, weight, and power requirements. A laser diode spectrometer based on wavelength modulation spectroscopy is being developed for this purpose by Vista Photonics, Inc. Two prototype devices were delivered to NASA Johnson Space Center (JSC) in September 2011. The sensors incorporate a laser diode-based CO_2 channel that also includes an incidental water vapor (humidity) measurement and a separate oxygen channel using a vertical cavity surface emitting laser. Both prototypes are controlled digitally with a field-programmable gate array/microcontroller architecture. The present development extends and upgrades the earlier hardware to the Advanced PLSS 2.0 test article being constructed and tested at JSC. Various improvements to the electronics and gas sampling are being advanced by this project. The combination of low power electronics with the performance of a long wavelength laser spectrometer enables multi-gas sensors with significantly increased performance over that presently offered in the EMU.

[1]Senior Research Engineer, 3 N. Chamisa Drive, Suite 1, Santa Fe, New Mexico 87508-9463.
[2]Research Engineer, 3 N. Chamisa Drive, Suite 1, Santa Fe, New Mexico 87508-9463.
[3]Principal Research Scientist, 3 N. Chamisa Drive, Suite 1, Santa Fe, New Mexico 87508-9463.
[4]President, 3 N. Chamisa Drive, Suite 1, Santa Fe, New Mexico 87508-9463, Member.
[5]Project Engineer, Space Suit and Crew Survival Systems Branch, Crew and Thermal Systems Division, 2101 NASA Parkway, Houston, TX 77058/EC5, Senior Member.
[6]Suit Systems Engineer, Systems Engineering Section, 2224 Bay Area Blvd., Houston TX 77058/JE2-1N.
[7]Project Engineer, Hardware Systems Project Engineering, 2224 Bay Area Blvd., Houston, TX 77058

Nomenclature

AC	=	alternating current
cm	=	centimeters
cm^3	=	cubic centimeters
COTS	=	commercial off-the-shelf
CO_2	=	carbon dioxide
EMU	=	extravehicular mobility unit
EVA	=	extravehicular activity
FPGA	=	Field Programmable Gate Array
JSC	=	Johnson Space Center
mmHg	=	millimeters of mercury
nm	=	nanometer
N_2	=	nitrogen
O_2	=	oxygen
PLSS	=	portable life support system
ppm	=	parts per million
psi	=	pounds per square inch
psia	=	pounds per square inch, absolute
RH	=	relative humidity
SBIR	=	Small Business Innovative Research
SMA	=	Subminiature version A
TEC	=	thermoelectric cooloer
VCSEL	=	vertical cavity surface emitting laser
VDC	=	volts, direct current
W	=	watts
WMS	=	wavelength modulation spectroscopy

I. Introduction

The infrared gas transducer used in the current space suit to measure and report the concentration of carbon dioxide (CO_2) in the ventilation loop during extravehicular activity (EVA) is approaching obsolescence. Next generation advanced portable life support systems (PLSS) require next generation breath gas sensing technology with performance beyond that in use on the extravehicular mobility unit (EMU). Accommodation within space suits demands that high-performance optical sensors meet stringent size, weight, and power requirements. Optical sensors based on laser spectroscopy are being developed for this purpose by Vista Photonics, Inc. Two prototype version 1.0 devices were delivered to NASA Johnson Space Center (JSC) in September 2011 (Fig. 1). The sensors incorporate a semiconductor laser-based CO_2 channel that also includes an incidental water vapor (humidity) measurement and a separate oxygen (O_2) channel using a vertical cavity surface emitting laser (VCSEL). Both prototypes are controlled with a low-power digital architecture. Based on the results of the initial instrument development, further prototype development and refinement were desired. Several improvements to the version 1.0 devices were implemented, and the upgraded version 2.0 devices were delivered to NASA in July 2012 (title page photo). The combination of low power digital control electronics with the performance of infrared laser optical measurements enables multi-gas sensors with significantly increased performance over that presently offered in the EMU.

Figure 1. Version 1.0 APLSS Optical Sensor. *The nearly cubic shape met the footprint requirements sought at the time of the development.*

Optical absorption spectroscopy provides signal that is linear and quantitative in concentration of the absorbing species for small absorbance. As expressed by Beer's law, the signal is directly

proportional to the concentration. wavelength modulation spectroscopy (WMS) and allows measurement of weak optical absorbance by shifting the detection band to high frequencies, where laser excess (1/f) noise is reduced, to achieve fractional absorption sensitivities near the shot-noise limit (10^{-8}) in the laboratory. Field measurements using WMS routinely attain minimum detection absorbances of 10^{-5} under extended operation. WMS offers a sensitivity enhancement over direct optical absorption spectroscopy of a factor between 100 and 1000.

To implement WMS, a small amplitude modulation at frequency f is superimposed on the laser diode injection current, which causes modulation of the laser wavelength because wavelength is tuned by changing the current. The amplitude of the current modulation is chosen so that the induced wavelength modulation is comparable to the width of the spectral feature under study. Absorption by the target gas converts the laser wavelength modulation to an amplitude modulation that induces alternating current (AC) components in the detector photocurrent. Phase-sensitive electronics are then used to demodulate the detector photocurrent at a selected harmonic, nf (typically, n = 2) (Fig. 2). By implementing this technique at sufficiently high frequencies, 1/f laser noise is reduced and, occasionally, detector-limited sensitivity can be achieved.

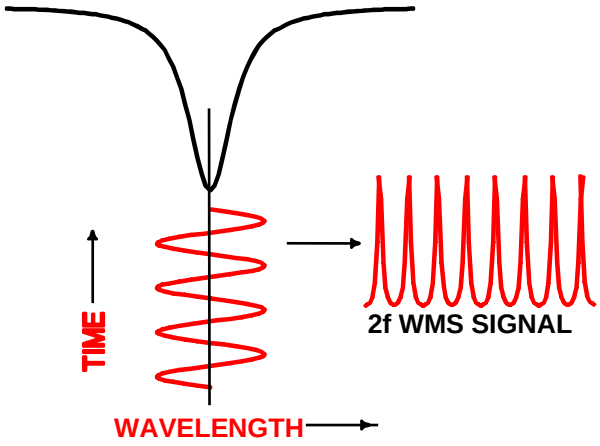

Figure 2. Generation of WMS signal. *Modulation of an optical source wavelength across the center of a molecular absorption feature produces WMS signal at twice the modulation frequency.*

The infrared wavelength range is well suited for both sensitive and selective detection of CO_2 and water vapor because many isolated absorption features are available for both species. Careful selection of the nominal wavelength range can even result in both species being detected with a single laser device. Whereas current modulation and second harmonic detection provide the basic absorption signal at a single wavelength, simultaneous current or temperature tuning the laser wavelength at a lower rate can produce either a single isolated absorption feature or an entire spectrum. Figure 3 shows the spectrum obtained for CO_2 and water vapor in the selected 2700 nanometer (nm) wavelength range along with a comparison to the HITRAN spectral database. The spectrum in the figure was obtained by slowly changing the laser temperature using a built-in thermoelectric cooler (TEC) over a span of about 30°C. Within the wavelength range produced by that scan, there are eight strong CO_2 absorption

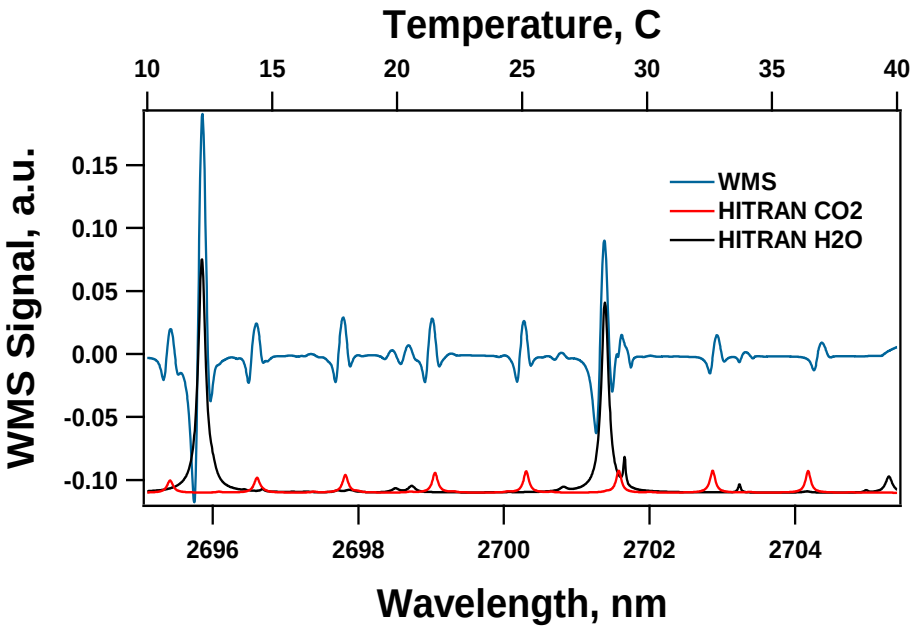

Figure 3. 2f WMS spectrum in 2700 nm range. *Ambient CO_2 and moisture absorption at 600 Torr for a 25 cm open path. The top axis shows how the laser wavelength is tuned with temperature.*

features and numerous water vapor lines of varying strength. The sensors for the APLSS application operate at the 2703 nm region where lines from both species can be accessed with a simple laser current ramp.

II. Optical Sensor Version 1.0

Many improvements had to be implemented to arrive at the final design of the version 1.0 sensors, and knowledge was borrowed from various Phase II Small Business Innovative Research (SBIR) projects. The result was an amalgam of optical approaches for the CO_2 and O_2 channels that, ironically, were not the ones originally demonstrated to the stakeholders at NASA JSC who ultimately funded the Phase III development. The contract was awarded in late May 2011 with breadboard prototyping conducted during May-July 2011. Integration and alpha testing occurred in August-September 2011, with prototype delivery of two units at the end of September (Fig. 1).

The challenge was to integrate the optical channels into a small rugged device that operates autonomously. This required a reduction in size of both originally envisioned optical layouts as well as all the associated electronics. Design integration and electronics reduction occurred over the course of 3 months. The version 1.0 sensors made some design concessions to meet the timeline. It was originally intended to provide the deliverable devices in a single enclosure, including both the main electronics and the optical sensor components. However, early on it was determined that the optical sensors should be kept separate from the electronics to the extent possible due to future accommodation in elevated O_2 environments. This would have also resulted in an enormous sample volume. An expeditious compromise was to simply co-locate both sensor channels into the same enclosed volume, but without the control electronics, for gas sampling at variable pressure. Consequently, the enclosed volume of 200 cubic centimeter (cm^3) was still much larger than required to simply house each channel separately. The black box on top in Fig. 1, with the electronic feed throughs, houses both of the optical channels.

The electronics architecture in the 1.0 devices is comprised of one main analog board, a Field Programmable Gate Array (FPGA) board, and a microcontroller. Design of the main analog board was straightforward after drawing on the experience acquired in a Phase III development of Vista Photonics' Optical Life Gas Analyzer (OLGA), which runs four independent laser channels. The function of the main analog board is to provide current drive capability for both laser channels and control their associated TECs. An additional TEC circuit is used to control the photodetector temperature for the CO_2 channel. The main board also routes power to the FPGA and microcontroller boards and two small photodetector preamplifiers. The optical enclosure dictated the size available for the electronic footprint after it was decided to stack the electronics underneath the box. Reduction in the number of laser channels made this simple for the main board. Reduction in the footprint of the FPGA was more of an effort because only commercial off-the-shelf (COTS) devices had been used up to that point. Nonetheless, the design task was accomplished in the time allotted. Fig. 4 shows the custom-designed FPGA board on the left alongside the COTS device on the right. A significant reduction in footprint was realized; the custom FPGA board is designed to plug directly into the main analog board through a single connector. The custom board eliminates many of the conveniences associated with the COTS board but is able to essentially run the programs developed with the COTS device. Thus, sensor set-up is accomplished by determining the required parameters with the more flexible COTS device and then burning the specific program onto the smaller custom device.

Figure 4. Custom and COTS FPGA. *Reduction of the electronics footprint was enabled by using the custom FPGA board in the left of the photograph.*

Figure 5 presents the combined main analog board and custom FPGA board in the deliverable devices after removal of temporary hardware including an LCD and control buttons. The microcontroller is not attached in the figure; the sensor is shown alongside the electronics dust cover and upside down. The two staggered square boards in the foreground are photodetector preamplifiers. The gas sensor enclosure is on the bottom. An RS-232 communications interface is provided via the coaxial Subminiature version A (SMA) cable, which routes to a serial-to-universal-serial-bus interface for connection to a netbook computer running an executable LabView VI. A momentary switch disables the lasers before power down.

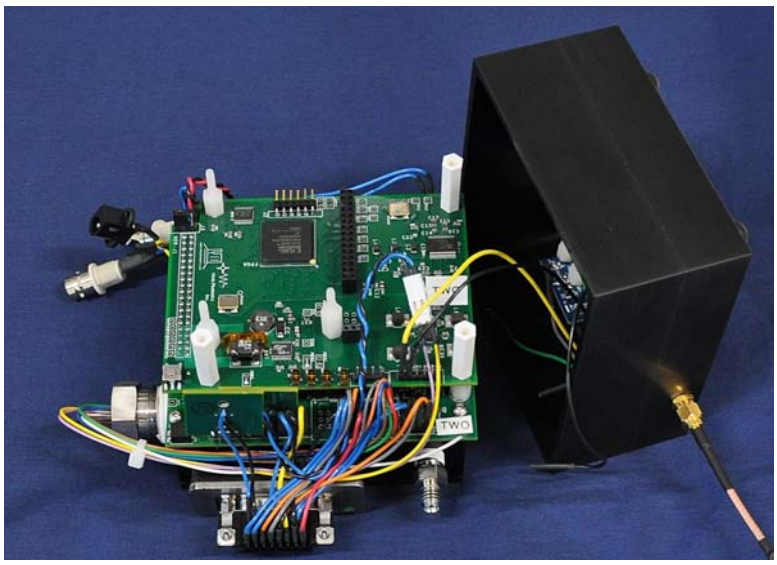

Figure 5. Sensor version 1.0 electronics. *The custom FPGA board plugs directly into the main analog electronics board that controls the lasers. The optical sensors are in an enclosure underneath. A plastic dust cover protects the electronics.*

The original design for the CO_2 channel was an optical path length enhancement approach using VCSELs at 2004 nm based on Vista Photonics' EVA Phase II SBIR development with NASA Glenn Research Center. This was the architecture originally demonstrated at NASA JSC that eventually led to the Phase III project. However, it was determined that using a laser diode at 2703 nm in a simple short optical path offered numerous advantages, including wider dynamic range and the potential for a smaller sample volume. Higher performance than achieved in the EVA Phase II was expected, and demonstrated, by using these laser diodes at 2703 nm rather than the VCSEL devices at 2004 nm due to the much higher absorption cross sections at the longer wavelength. Expertise with that wavelength already existed from a separate Phase II SBIR contract to develop a compact CO_2 sensor for unmanned aerial vehicles with NASA Goddard Spaceflight Center. In contrast, the O_2 channel did indeed use the path length enhancement approach originally proposed for CO_2. This was not an issue for O_2, where sample volume and response time were less of a concern. This remains the case for the two channels. Because the sensor channels in version 1.0 are collocated in the pressure tight enclosure that mounts to external control electronics, the control electronics are not in contact with the sample gas. Nonetheless, some electronics remain inside the enclosure including the two semiconductor lasers, two photodetectors, and a pressure sensor.

The sensors are fully self contained and run independently with simple 6 volts, direct current (VDC) power, drawing slightly less than 2 watts (W) on average. The FPGA and main boards are capable of running the sensor, acquiring the raw data, and converting it to properly demodulated WMS signal. However, they do not provide data analysis, calibration, data logging, or external communication. The microcontroller is essential for providing those functions. A commercial unit was retained in the deliverables.

A. Carbon Dioxide and Water Vapor Channels

Alpha testing of the combined optical sensors for cross contamination and pressure, temperature, humidity dependence of CO_2 precision was accomplished in the vacuum tight optical sensor enclosure incorporating the open path CO_2/humidity channel at 2703 nm, the O_2 channel at 760 nm, and the onboard pressure sensor (small pcb). Gas inlet and outlet is provided by 1/8" compression tube fittings. A DB-15 connector is used to power the open path and pressure sensors. A 9-lead ½" NPT vacuum feed through powers the O_2 sensor channel. The enclosure volume is about 200 cm^3 and was primarily determined by the need to accommodate the O_2 path length enhanced cell. A single channel CO_2/humidity sensor would use a much smaller sample volume. Temperature is determined by an external thermistor located in a pocket drilled into the aluminum enclosure.

Extensive data were taken for CO_2 over a wide range of operating pressures and conditions. Somewhat less data were obtained for O_2 and water vapor due to time constraints in assembling the final devices. The 2703 nm wavelength range contains two absorption features for CO_2 with significantly different absorption cross sections (Fig. 6). Dynamic range requirements for CO_2 detection were, thus, accommodated by operating the sensors such that both strong and weak absorption features were accessible in a single laser current-controlled spectral scan, along with a companion water vapor feature. The strong feature is used at low CO_2 levels whereas the weak line takes over at high levels. At moderate CO_2 levels the two measurement smoothly transition from one line to the other. In this fashion, both low detection limits and wide dynamic range is accomplished for CO_2. Early data for the strong CO_2 line were obtained by flow dilution of 8 mmHg CO_2 down to 0 at a constant 400 Torr. The residuals to an exponential fit showed a deviation of less than 0.01 millimeters of mercury (mmHg) during this 24-hour measurement. Similar measurements for water vapor at around 17 % relative humidity (RH) returned a fit deviation of about 0.05 mmHg, or about 0.2 % RH at 25°C.

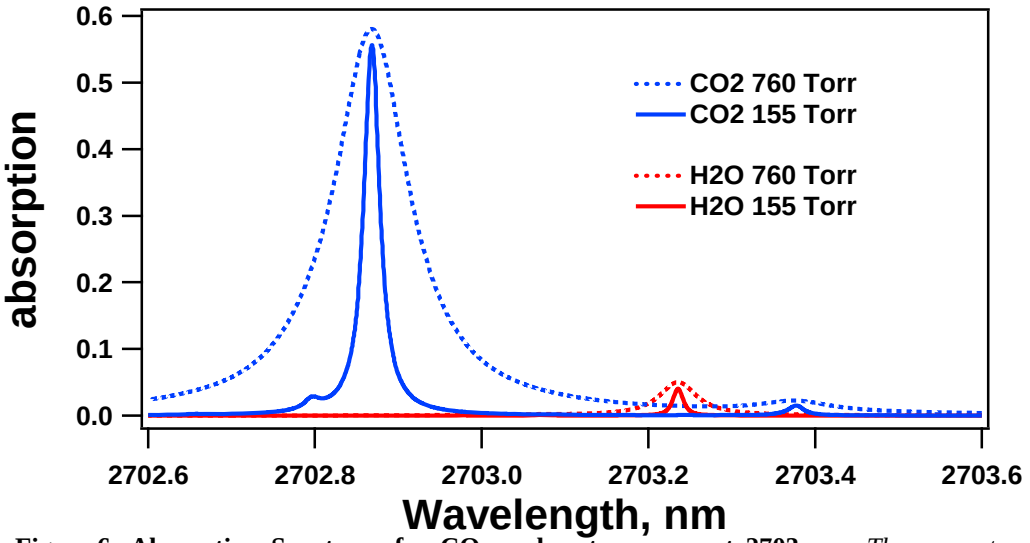

Figure 6. Absorption Spectrum for CO_2 and water vapor at 2703 nm. *There are two carbon dioxide lines of different strengths and a water vapor line in the CO_2 channel. The absorption linewidths for the lines are highly pressure dependent.*

The CO_2 channel in the version 1.0 sensor operates in the 2700 nm wavelength range with an open optical path of about 4 centimeters (cm). Optical absorption spectroscopy provides signal that is linear and quantitative in concentration of the absorbing species *for small absorbances*. As expressed by Beer's law, the signal is directly proportional to the concentration. However, over the range of levels encountered in the PLSS application, the strong line will enter into a non-linear regime of signal versus concentration. Using both absorption features does not entirely eliminate this non-linearity due to the relatively high concentration where the strong line hands off measurement responsibility to the weak line. Figure 6 also shows how the width of the individual absorption features are affected by changing total pressure. The lines get broader as the pressure increases. Version 1.0 sensors were calibrated from 150 Torr up to 800 Torr. Since the WMS measurement technique is sensitive to the absorption line width and the employed current modulation depth, the measured raw signal is necessarily affected by changing pressure. The sensors did not use the onboard pressure measurement to adjust the laser modulation depth to mitigate pressure effects. This would have been very difficult to implement in such a short time because it requires bidirectional communication between the FPGA and the microcontroller. Instead, the measured pressure was simply used to correct the measurement error upon deviation from the single pressure where the sensor was calibrated for unity correction (429 Torr, 8.3 pounds per square inch (psi)).

Calibration of the strong CO_2 feature was quite complex with quadratic to cubic fits required at individual pressures over the span of concentrations. A range of seven pressures from 155 Torr to 760 Torr was employed. The fits to the raw data are shown in Fig. 7. Individual calibration curves were required for each deliverable sensor since the curve is a function of modulation depth, which is difficult to set identically for both devices. In Fig. 7, the curvature in an individual fit is due to the non-linear relationship of absorption signal and CO_2 concentration at high levels. The lowest trace is that for 760 Torr (the modulation depth was optimum at 100 Torr). Thus, the lasers are very undermodulated at high pressure, which degrades the generated signal. Note that the 0.04 fractional concentration (4% CO_2) at 760 Torr represents about 30 mmHg partial pressure (the highest level in the desired

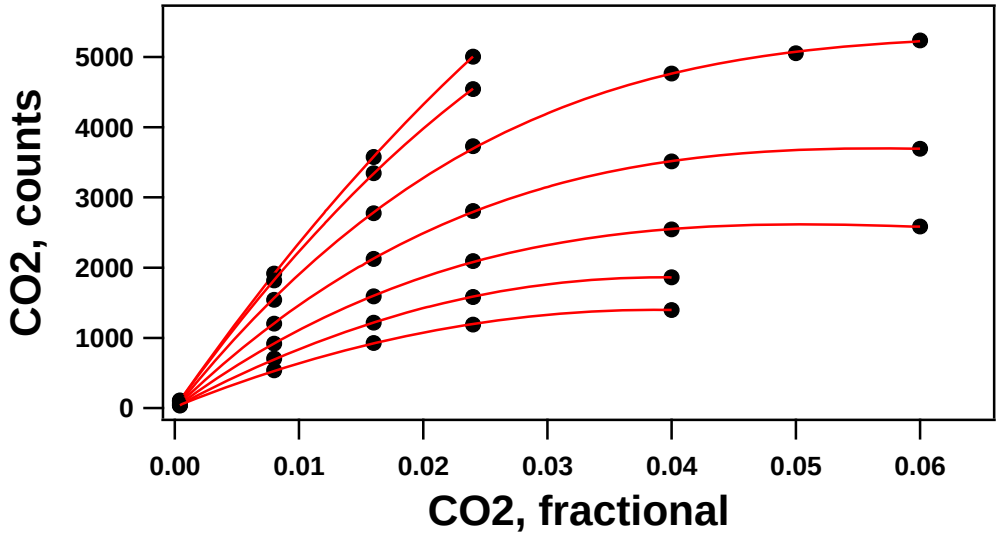

Figure 7. CO_2 Signal versus concentration for strong line at 2702.9 nm. *Signal for the strong line is non-linear with concentration at the highest levels where the weak line takes over. The measured signal is also a strong function of pressure which must be measured and compensated in the version 1.0 sensors.*

range). In Fig. 7, the reason the seven traces do not lie on top of one another is because the laser modulation depth was fixed and optimized for a single pressure even though the sensor pressure environment was widely variable. This results in less-than-optimum performance at any pressure that deviates from 150 Torr. Nonetheless, the version 1.0 sensor performance remained high across the entire range. If bidirectional communication between the FPGA and microcontroller could be achieved, the laser modulation depth could be adjusted as a function of pressure and only a single non-linear calibration curve would be required for the strong CO_2 line. This possibility was a major improvement to follow in the version 2.0 sensors.

The weak CO_2 feature was linear with concentration at each pressure over the span of concentrations employed even up to 20% CO_2 at 155 Torr (30 mmHg CO_2 partial pressure) but still required a separate fit at each pressure. In the case of both CO_2 absorption features, the fit coefficients were calibrated as a function of pressure. Thus, the pressure measurement is used to obtain the individual appropriate calibration coefficients for both the weak and strong absorption features whether those are linear, quadratic, or cubic. The raw count data are then converted to concentration via those coefficients. In this way, the data analysis and conversion is reduced to two polynomial

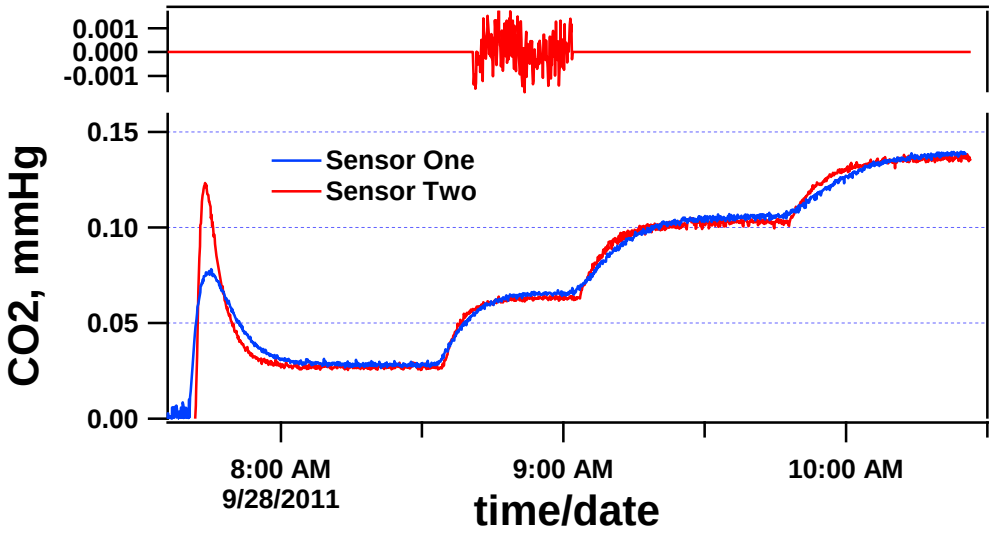

Figure 8. Calibrated CO_2 Signal from both version 1.0 sensors. *At low concentrations the strong CO_2 line offers high sensitivity and high precision. Both sensors are in close agreement after calibration immediately prior to delivery.*

operations and allows prediction of the fit coefficients outside the bounds of the pressures actually measured. These fit accuracies could be continually improved with more extensive data over a greater range of pressure and concentration alongside finer steps within those ranges. The version 1.0 sensors had not been calibrated for variable temperature by the end of the project, though that would have been straightforward; therefore, their accuracy was degraded at temperatures that deviated from about 23°C.

Figure 8 demonstrates that the early high performance predicted and demonstrated with the loose bread boarded components including the commercial FPGA has been preserved in the fully integrated deliverable units (note the date in the figure is the day before the units were shipped). The standard deviation of the CO_2 measurements using the strong absorption feature was better than 0.001 mmHg at low CO_2 concentrations at 310 Torr. Precision is somewhat better at lower pressures and somewhat worse at the higher pressures (0.003 mmHg at 760 Torr) because of the drop off in signal from the described fixed modulation depth. Similar performance was obtained for both deliverable devices. Both sensors presented essentially equal measurement precision under the same conditions, but also the measured signals were in good agreement and accurate. The signal from both sensors for several equal concentration steps where the strong line output is still in the linear regime are shown in Fig. 8. There is close agreement between the two devices. The signal response from sensor two was delayed from sensor one because the gas sample flowed sequentially from sensor one to sensor two in a daisy chain configuration. The inherent sensor response for both devices was from 10% to 90% within 10 seconds.

B. Oxygen Channel

There are two regions on either side of 762 nm for detection accessible with available VCSEL devices. The APLSS O_2 sensors use lasers operating around 760.6 nm. As with the CO_2 channel, WMS with second harmonic lock-in detection produces absorption spectra with qualitative second derivative lineshapes. Figure 9 shows the spectrum obtained for O_2 by tuning the laser wavelength with temperature as shown previously for CO_2. The black trace shows the spectrum simulated from the HITRAN database. The VCSEL devices tune much farther for a given change in temperature. The tuning rate with current is likewise much faster than that of laser diodes. This results in much less amplitude modulation associated with the desired wavelength modulation, making O_2 detection easier.

Figure 10 shows data obtained from the path length enhanced O_2 sensor as a function of pressure, before pressure correction was added prior to delivery. The enhanced path length equates to about 150 cm in a sample cell less than 4 cm across. At the higher pressures, O_2 signal is higher with a standard deviation of about 0.2 %.

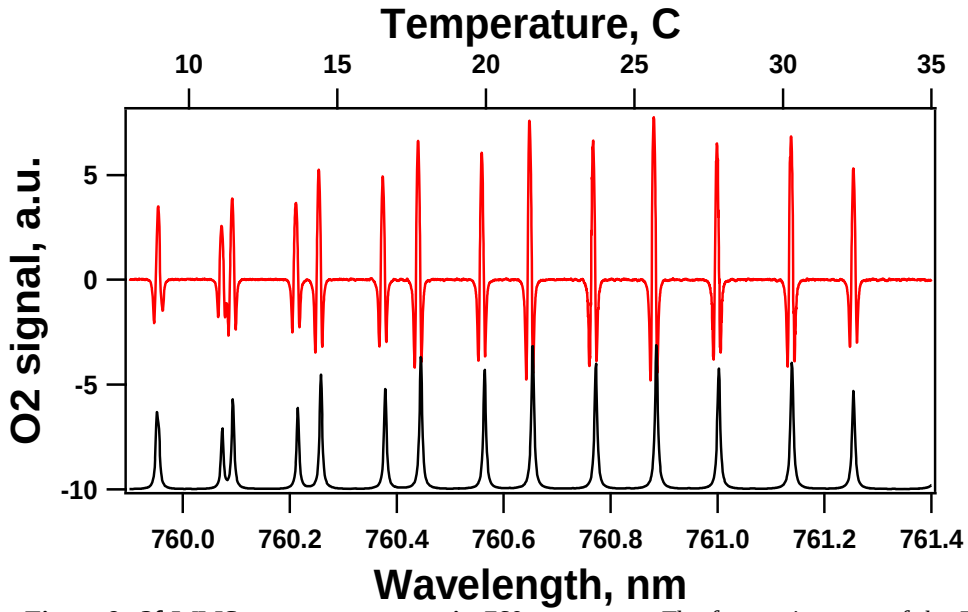

Figure 9. 2f WMS oxygen spectrum in 760 nm range. *The fast tuning rate of the 760 nm VCSELs allows access to many suitable absorption features for oxygen. The line at 760.68 nm is used in the APLSS application.*

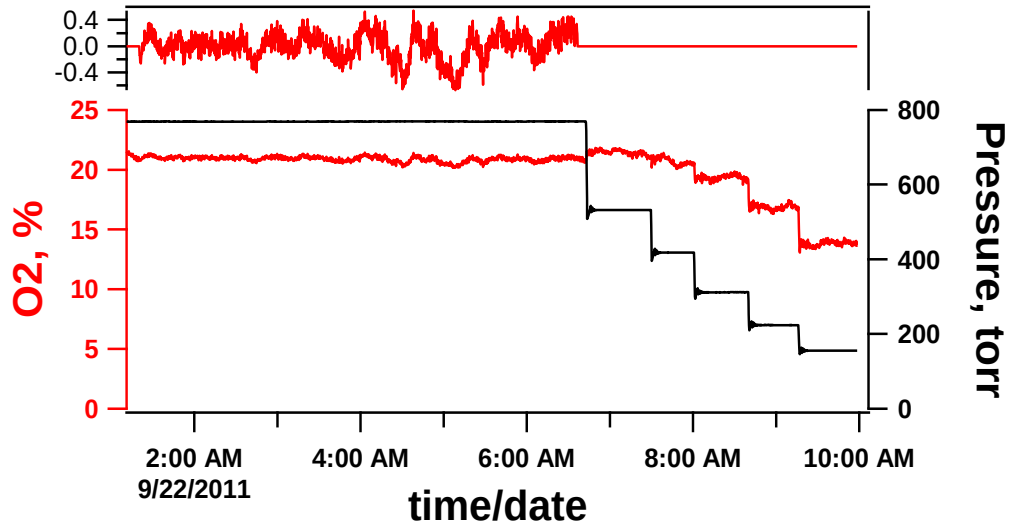

Figure 10. Calibrated O_2 Signal before pressure correction. *Oxygen measurement precision is about 0.2 % at sea level. The signal changes predictably with lower pressure and is easily compensated in the version 1.0 sensors.*

This is about 2 times worse precision than expected, given like experience with similar sensor cells using COTS electronics. The difference is likely attributable to excess noise in the custom-integrated electronics that sought to drive both high power DFB lasers for CO_2 alongside low power VCSEL devices for O_2 in a highly space-constrained arrangement. However, the noise is still high when the CO_2 channel is deactivated. This may indicate that the noise is being picked up from the FPGA modulation signal for CO_2, which is not easily deactivated. It is expected that further development of the custom electronics will improve performance to about 0.1 % O_2 concentration.

C. Unit conversion and calibration using Netbook computer

At the time of the version 1.0 sensor delivery, the species calibrations for all three gas channels were employed through the use of a netbook computer to take the raw sensor output in counts over a serial port and convert to concentrations. The netbook also logs appropriate converted data along with temperature and pressure data. It has since proven feasible to incorporate the calibrations directly into the microcontroller such that the output is in concentration instead of counts for each gas. With some hardware changes, those measurements could also be communicated with simple voltage proportional outputs for each gas. However, the sophistication of the emerging APLSS 2.0 test article is more than capable of using the digital serial output, which is more accurate by eliminating a digital-to-analog conversion within the instrument followed by an analog-to-digital conversion by the end user. The two version 1.0 sensors are shown with netbook computers reporting the measured gas concentrations in Fig. 11 immediately prior to delivery.

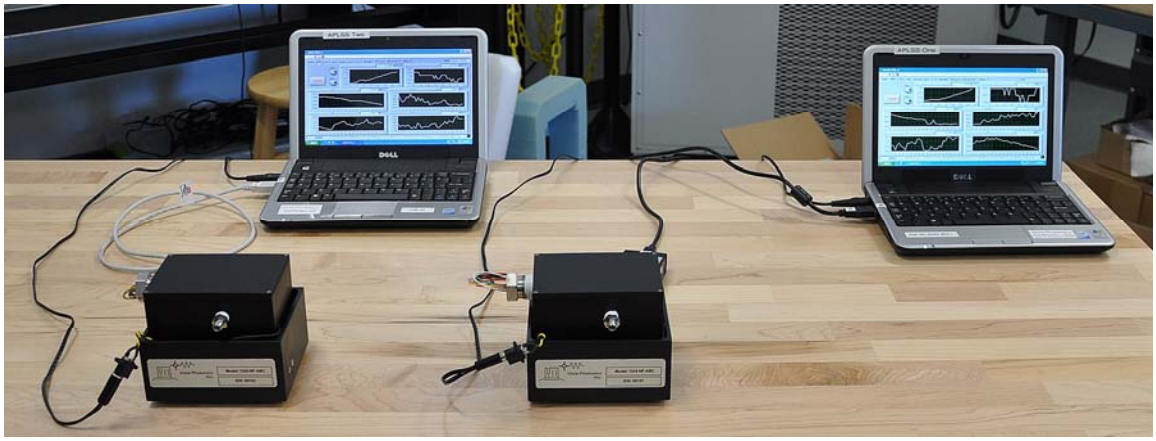

Figure 11. Version 1.0 sensors before delivery. *Both sensors offer equivalent performance for the three gases measured. Netbook computers were required to implement the complex calibration in the version 1.0 sensors. The computers were not simply logging data, they converted the raw engineering units into useful concentration data after acquiring pressure readings from the onboard sensors.*

III. Optical Sensor Version 2.0

The version 1.0 sensors were installed and tested in the APLSS 1.0 bread board in October, 2011. Good measurement agreement with several other CO_2 sensors accessible on the bread board was achieved over the course of several days with Vista Photonics' personnel participating. This testing occurred after the primary demonstration of the APLSS 1.0 breadboard and before transition to the present 2.0 version. Several changes that would improve the devices were highlighted by this testing. It was learned that the pressure sensor inside the optical enclosure was susceptible to failure at the high humidity levels encountered. Since the APLSS will employ its own state-of-the-art pressure sensor, the version 2.0 optical sensors use this measurement communicated over a serial interface instead of using a separate onboard pressure sensor. However, a better pressure sensor was implemented in the version 2.0 sensors as a precaution should onboard measurement become necessary in the future.

A second desired improvement was to separate the O_2 and CO_2 channels from inside the same enclosure sample volume. Oxygen sensing with the path length enhanced architecture is the determining factor in the 200 cm^3 volume of the optical sensor enclosure. The open path CO_2 channel was built as a sub-assembly and then mounted inside the optical sensor enclosure. The enclosure simply functions as a small vacuum chamber and sample cell. The enclosure was added due to the need to separate the main electronics from the optical sensors, which are to be in contact with the sample gas. Even so, the sensors themselves require electrical wiring for the laser and photodetector and this wiring is in contact with the sample gas. The CO_2/humidity sensor alone could present a significantly reduced footprint and 2 cm^3 volume if separated from the O_2 channel, which would itself only occupy 50 cm^3. The common enclosure also exposes the laser diode, VCSEL, and photodetectors to what could eventually be a pure O_2 environment. The version 2.0 sensors locate the electrical leads for the laser diode, VCSEL, and the photodetector for the CO_2 channel outside of contact with the sample gas. Only the electrical leads of the photodetector for the O_2 channel remains in contact with the sample gas and they carry only about 30 microwatt.Figure 12 shows the version 2.0 sensors being transitioned from the earlier 1.0 sensors. The original delivered 1.0 devices were returned for

upgrade to the new 2.0 version in March 2012, and the new devices delivered in July 2012. Several of the improvements are evident in the figure. The aluminum block in the center foreground is the new CO_2 and water vapor channel with both the laser diode and photodetector removed from contact with the sample gas. The new O_2

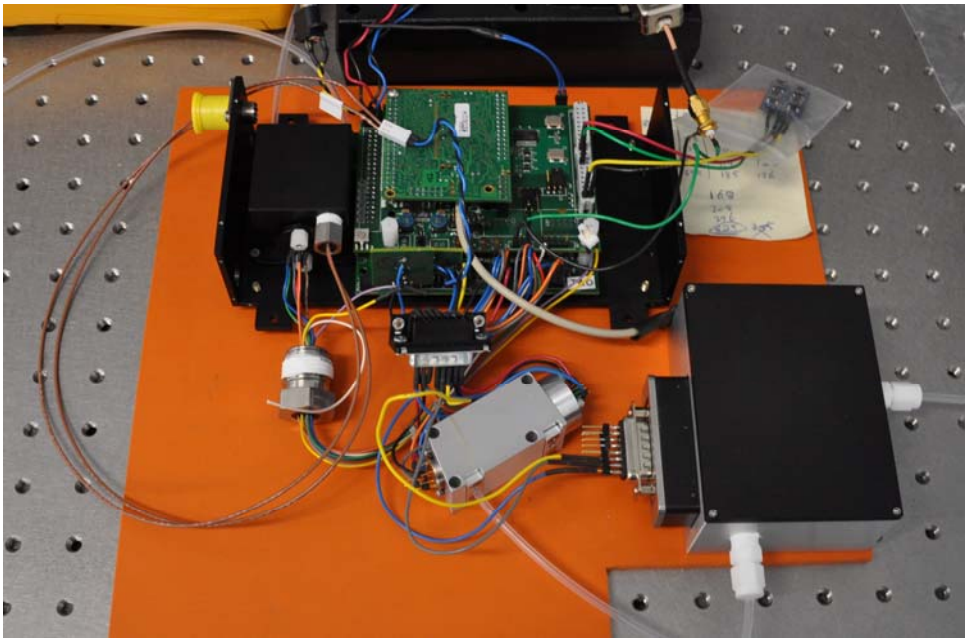

Figure 12. Transition and upgrade of version 1.0 sensors to version 2.0. *The photograph shows a transition period where the new 2.0 optical channels are running from the old version 1.0 electronics. An old 1.0 enclosure is used just for pressure measurement. It remained only to acquire the new electronics to complete the hardware portion of the upgrade to version 2.0.*

Figure 13. Integrated Version 2.0 sensor. *Optical and electronic layout after full conversion to 2.0 architecture. An RS-485 bi-directional interface and power supply board compatible with the APLSS 2.0 system has been added.*

channel is in the cubic enclosure on the upper left of the figure with the vacuum electrical feed through. The other wires on the enclosure are for the VCSEL, which is located out of contact with the sample gas. The sensor volume has been rearranged for accommodation within the available space of the APLSS 2.0 system. This resulted in a more rectangular shape than the previous cubic shape of the 1.0 devices. Additional changes involved locating a single

electrical connector and both gas line connectors (inlet and outlet) on the same side of the sensor enclosure. The gas connectors were custom made to transition from the APLSS-preferred style to the compression tube fittings used inside the sensor. Upgraded electronics were also produced during that period before delivery of the version 2.0 sensors that included a new main analog board and a redesigned custom FPGA board. One of the photodetector preamplifiers was also relocated onto the main analog board. The RS-232 interface already on the microcontroller board was connected through a new custom RS-485 interface offering bidirectional communication. This allows sending of multiple commands to the sensor as well as providing for an external pressure measurement. The microcontroller has been, likewise, upgraded to eliminate an unnecessary compact flash card reader. The version 1.0 sensors operated off of a 6 VDC power supply whereas the upgraded 2.0 sensors operate from the APLSS supplied 16 to 34 VDC power. That power conditioning was added to the same board containing the RS-485 interface. Figure 13 shows the version 2.0 sensor after integration of the physical improvements.

In addition to the reduced sample volume, increased safety, and upgraded electronics, improved sensor performance was realized by making the laser diode modulation depth a pressure-dependent variable. The 1.0 sensors operated with a fixed modulation depth (wavelength excursion turning points) although the absorption linewidth is a function of pressure. Consequently, signal is degraded at pressures other than the one for which the sensor is optimized. Figure 14 shows how the signal changes with pressure for a fixed modulation depth. Of course, the calibration takes care of this in terms of the concentration reading reported to the end user. However, the calibration cannot retrieve the lessened performance (reduced precision) for pressures where the modulation depth is not optimal. Such variation can approach a factor of three worse precision at the highest pressures. The figure also shows the sensor readings for the case where the modulation depth is optimized for the actual pressure. Very little variation is found, which would greatly reduce the computational overhead employed in the version 1.0 sensor pressure compensation (which was complex enough to require the netbook computer). A variable modulation depth based on the onboard pressure reading or an external measurement would essentially eliminate the sensor pressure dependence. Thus, the raw sensor output would be nearly pressure independent, requiring little clean up from the calibration algorithm. This approach would require the FPGA to employ a feedback loop of modulation depth based on the pressure sensor reading. Vista Photonics had not employed this approach before on an autonomous sensor and appropriate safeguards to protect the laser diode were developed.

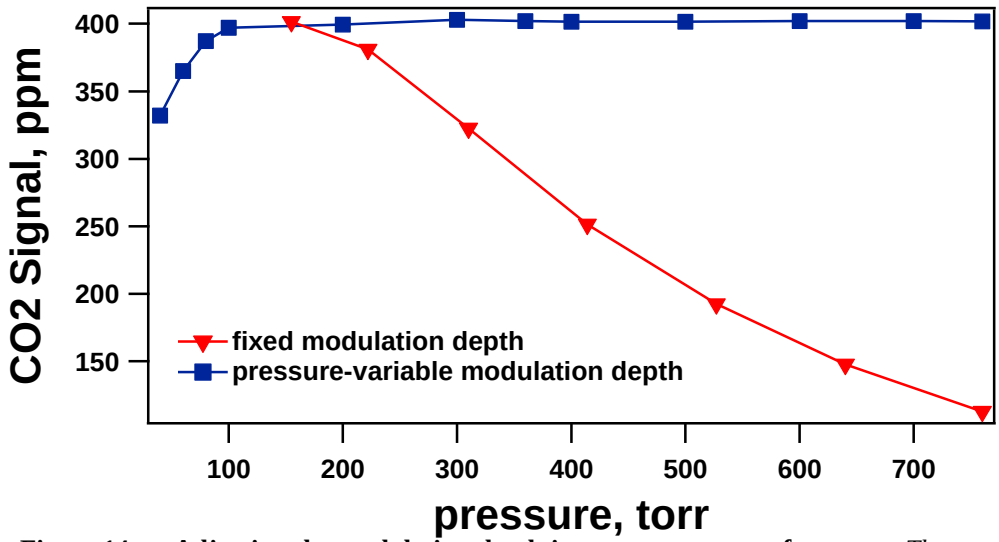

Figure 14. Adjusting the modulation depth increases sensor performance. *The version 1.0 sensors simply corrected for pressure variation away from the optimized level as shown by the fixed modulation depth trace. Sensor performance dropped off away from the optimum pressure. In contrast, the version 2.0 sensors adjust their operation as a function of pressure to maintain their high performance across the entire required pressure range.*

Figure 15 shows how the modulation depth has to be changed to keep the CO_2 signal as constant as possible under changing pressure conditions at a fixed mole fraction (parts-per-million by volume). Note the signal drops if the pressure is less than 200 Torr, even with optimized modulation depth as the line goes from primarily pressure broadened to Doppler broadened. The line doesn't narrow up and increase in height for pressures below 200 Torr. The limit requirement for the sensors is 150 Torr, so the data will have some error, if left uncorrected, at the very

lowest pressures by the microcontroller where a tiny bit of precision will be lost. However, the sensors were previously optimized for 100 Torr in Phase III so that at every higher pressure the signal had degraded precision. Thus, the upgraded version 2.0 sensors will have higher precision at every pressure at which they operate. The data of Fig. 15 were used to construct the required modulation depth versus pressure in a fully closed loop control such that the system would take the known pressure and adjust the modulation depth automatically. The microcontroller informs the FPGA of the pressure, and the FPGA uses the information to drive the laser diode, or VCSEL, appropriately. Full bidirectional communication has been implemented between the two digital devices. The version 1.0 sensors had unidirectional communication only. This was the most complex task for implementing the desired version 2.0 improvements. Figure 16 shows the results of that implementation where the pressure was scanned from 150 Torr to 800 Torr with fully automated control of the modulation depth. Note the only small variation in CO_2 signal at the fixed 13,600 parts per million (ppm). The small oscillations in the fit residuals are probably due to the limited number of data bins in the spectrum and can likely be corrected with a second order adjustment of the modulation depth, which is being investigated for future improvements. Note that the error is still only about 0.02 mmHg at the lower pressures and 0.01 mmHg at the higher pressures. The two upgraded sensors are shown in Fig. 17 prior to delivery in July 2012.

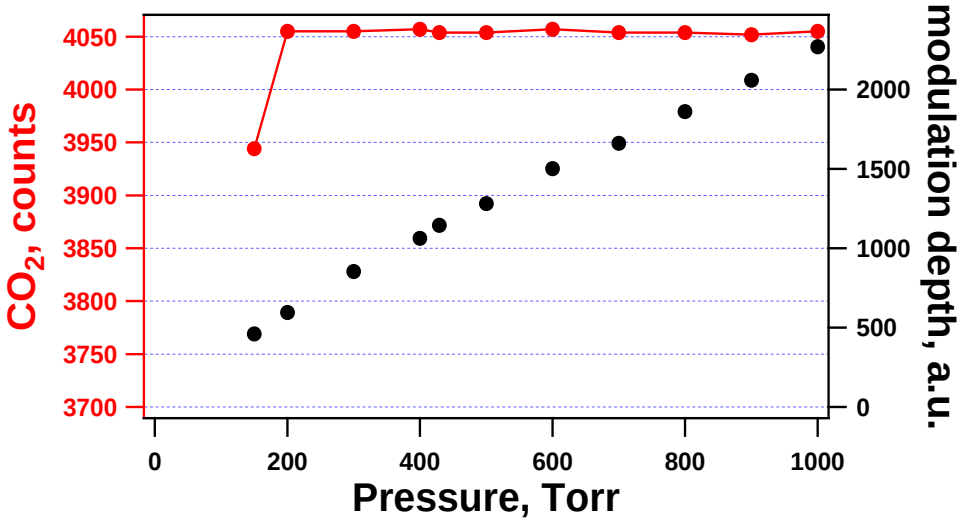

Figure 15. Modulation depth adjusted as a function of pressure. *By adjusting the operation of the lasers as a function of measured pressure the sensor raw output signal is essentially independent of pressure, greatly simplifying calibration.*

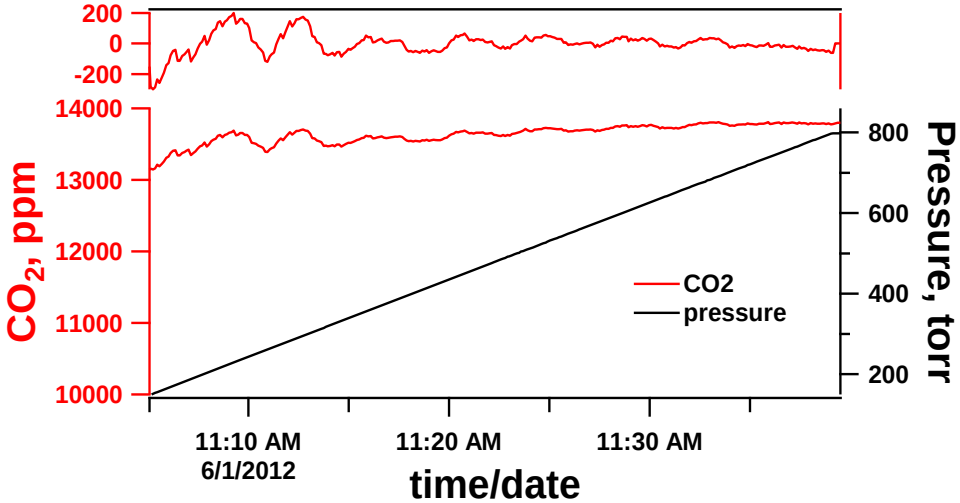

Figure 16. Version 2.0 sensor signal with changing pressure. *After implementing the modulation depth tracking with pressure, the calibrated sensor reading shows little variance over a wide pressure range.*

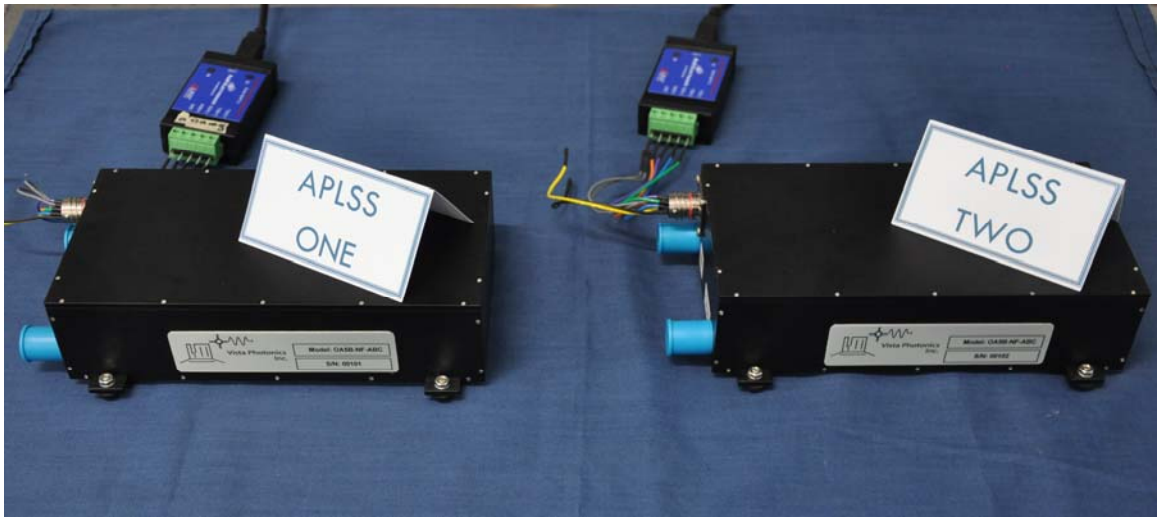

Figure 17. Version 2.0 sensors before delivery. The two version 1.0 sensors were upgraded to version 2.0 and are geometrically and electrically compatible with the APLSS 2.0 system.

IV. Gas Sensor Test Rig

The Vista Photonics, Inc. optical breath gas sensors (both version 2.0 sensors) will be tested on the Gas Sensor Test Stand shown in Fig. 18. The schematic of the Gas Sensor Test Stand is shown in Fig. 19. The test stand was designed and built by the Space Suit and Crew Survival Systems Branch at NASA JCS for testing and characterizing the performance of gas sensors for PLSS. The test stand provides a fully automated capability for delivering a gas mixture of controlled nitrogen (N_2) and CO_2 concentrations (by mass), mixture static and dew-point temperatures, and mixture mass flow rate to a gas sensor under test. Additionally, the stand contains a vacuum chamber in which the sensor resides during test, which allows for testing of the sensor at the typical sub-ambient static pressures and pressure differentials under which PLSS gas sensors are expected to operate. Closed-loop pressure controllers maintain a desired internal sensor pressure with respect to sensor ambient during test to replicate the range of gas densities encountered during PLSS operations. The test stand provides fully automated control, monitoring, collection, and logging of all test stand and sensor operational parameters and data, and also protects against over-pressurization, over-voltage, and over-current conditions. Lastly, a Picarro Gas Analyzer is used to provide verification of the CO_2 concentration being delivered to the gas sensor under test. Table 1 provides a listing of key test stand instrumentation.

Figure 18. Gas Sensor Test Stand

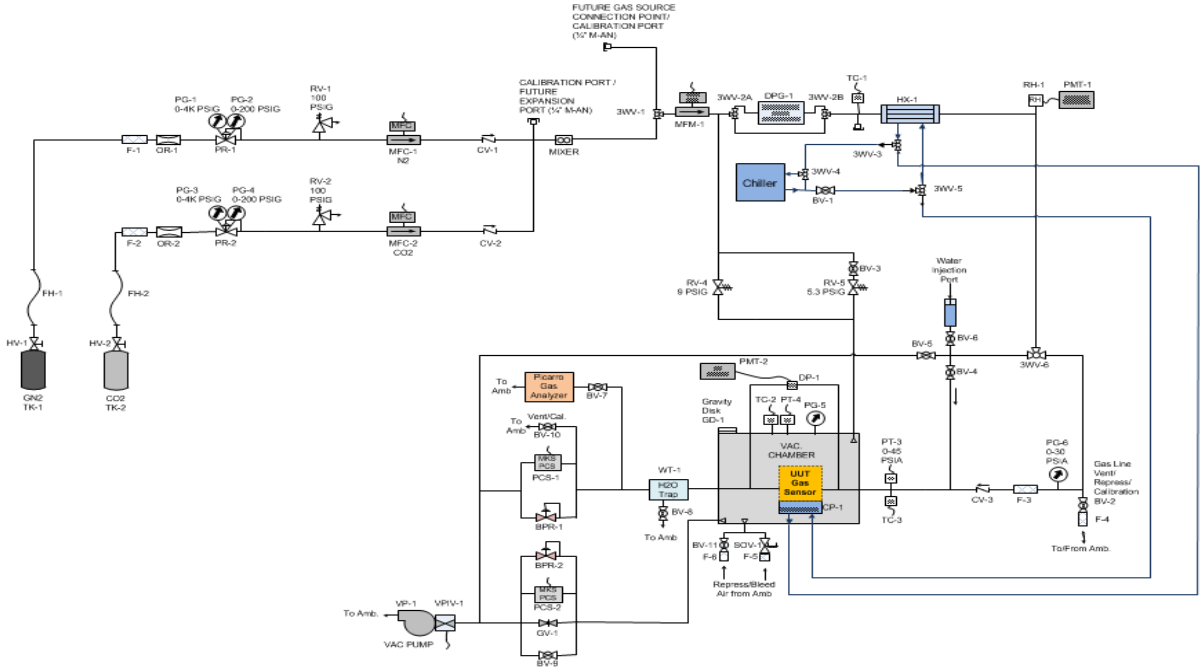

Figure 19. Gas sensor test stand schematic.

Table 1. Gas Sensor Test Instrumentation

Instrument	Manufacturer	Description	Purpose
PT-3	Paroscientific	0-45 psia pressure transducer	Measure pressure of the system
RH-1	Vaisala	0-100% RH, -40 through 180°C, humidity and temperature sensor	Measure relative humidity and temperature of the gas stream
TC-3	Omega	425°F Thermocouple	Measure temperature of gas stream
DPG-1	Li-COR	0-50°C Dew point generator	Control humidity injection
PCS-1	MKS	0-2000 Torr pressure controller	Control internal pressure of the test article
PCS-2	MKS	0-2000 Torr pressure controller	Control chamber/ambient pressure on test article
MFC-1	MKS	0-5000 sccm N_2 mass flow controller	Control N_2 injection rate
MFC-2	MKS	0-200 sccm CO_2 mass flow controller	Control CO_2 injection rate
MFM-1	MKS	0-2000 sccm 1%CO_2/N_2 mass flow controller	Measure flow rate of gas mixture
DP-1	MKS	0-5 inH_2O differential pressure transducer	Measure differential pressure across the test article
VP-1	Varian	0-250 lpm pump speed Triscroll pump	Provide sub-ambient internal and ambient static pressures.
CHILLER	Thermo Scientific	-10 to +80°C (14-176°F) Cooling/heating chiller	Regulate temperature of cold plate or heat exchanger
PT-4	Kurt J. Lesker	$1X10^{-4}$ through $1X10^{+3}$ Torr	Measure pressure of chamber
PICARRO	Picarro	Gas Analyzer	Provides verification of CO_2 concentration of gas mixture
RV-1, RV-2, RV-4, RV-5	Circle Seal Controls	Over-pressure relief valves	Protect sensor under test and test stand instrumentation from over-pressurization
PS-0	Agilent	DC power supplies	Provides power and over-voltage and over-current protection for test stand instrumentation and for the test article

V. Conclusion

An integrated optical architecture using lessons learned and techniques advanced on several NASA SBIR projects has been developed for use in the emerging advanced PLSS for EVA. The first version of the sensors proved the value of the optical approaches employed and resulted in a compact, rugged design. Various design improvements were made in the second version that provided a more suitable geometry for the EVA application while increasing sensor performance. Sensor power draw was also reduced and full bidirectional communication added in the second version. Further, the complex calibration previously done through a netbook computer has been offloaded onto the internal microcontroller. The serial communication is now used primarily to acquire the concentration data. In future work, a version 3.0 sensor design already in progress could see a nearly 30% decrease in length and volume by better geometric coupling of the CO_2 and O_2 channels.